Feasibility study on low-resolution uncooled thermal imagers for home-security applications

Tzong-Sheng Lee*
Jin-Shown Shie, MEMBER SPIE
National Chiao Tung University
Institute of Electro-Optical Engineering
Hsinchu, Taiwan
E-mail: 850374@itri.org.tw

Abstract. The feasibility of using low-resolution thermal imagers for home security applications is analyzed, taking low cost as the primary consideration. The smallest possible sensor size and resolution are chosen as the operative criteria and derived by simulation, in accordance with the optical constraints of a general home security system and the minimum target feature recognizable using image processing. Low-resolution simulated thermal images were generated by downgrading the high-resolution images captured by an uncooled IR camera, through sampling and modification. Caricatures of human beings and family pets are extracted for recognition using aspect-ratio and neural network methods, which are compared with one another for detection probability. It is demonstrated that highly reliable detection of human beings or pets with a minimal target feature of 8×8 pixels can be obtained using the neural network method. Also, a fire can be detected early using its temporal size variation and higher temperature. Finally, low-cost fabrication of the proposed low-resolution passive infrared imaging system with an uncooled FPA sensor utilizing a fully standard application-specific IC CMOS process is also discussed in detail. [S0091-3286(00)02706-9]

Subject terms: passive IR sensing; home security; thermal imager; uncooled camera.

Paper 990126 received Mar. 22, 1999; revised manuscript received Nov. 4, 1999; accepted for publication Dec. 6, 1999.

1 Introduction

Many kinds of sensor systems are in use in home security systems. They generally provide two main functions: intruder and fire detection.[1–7] No current system can satisfy both functions completely. In addition to contact, vibration, proximity, ultrasound, and microwave sensors, passive infrared (PIR) motion detectors are the most popular at the present. PIR motion detectors have the capability of sensing warm subjects volumetrically over the entire surveillance zone.[3] However, the current PIR detectors, dual- or quad-element pyroelectric types,[4] are imperfect in target identification because they cannot provide an image of the detected target, even if they are combined with microwave or ultrasonic sensors.[5] A CCTV[6] monitoring system can provide a target shape, but a low-cost system cannot work effectively in the dark without active illumination. This excludes commercial CCTVs from long-distance applications without the addition of extra lighting and cost. The active CCTV technique is also ineffective for the early detection of fire, which is essential for home security.[7] These problems can be solved ideally using a passive thermal imager, if the cost issue can be settled.

Recently, the dramatic development of uncooled IR thermal detectors, using surface-micromachining technologies,[8–10] has reduced the cost of thermal imaging sensors drastically in comparison with cryogenic quantum-type sensors.[11] The manufacture of monolithic thermal-type IRFPA detectors is now possible in silicon IC foundries,[12–15] taking advantage of their voluminous processing capabilities. This has led to the price of a thermal imager system dropping from tens of thousand dollars a few years ago to an expected few thousand in the near future.

As a result of this reduction in cost and the efficient operation of uncooled IRFPA imagers, it is expected that the opportunities to employ passive infrared sensing technology will greatly increase in common applications,[16,17] such as fire detection and security. However, for home security applications, there are still some problems to overcome. First, the price of current high-resolution uncooled thermal imagers is still beyond what typical families can afford. Second, the millions of bits of high-resolution image data coming from many thousands of systems, if transmitted asynchronously through networks to a security center, might overload the center. This then raises the question: what is the lowest required resolution for common targets, such as are expected to appear in a typical house, to be reliably recognized using PIR image detection? The most common targets are human beings, family pets, and fire.

In this article, the system specifications for a general PIR home security system are considered, based on the use of an uncooled thermal sensor that can work effectively with minimal size. For simulation, various low-resolution thermal images can be artificially generated from the images obtained by a commercial high-resolution thermal im-

*Present address: Microsystems Technology Division, Microsystems Laboratory, ITRI, Taiwan.

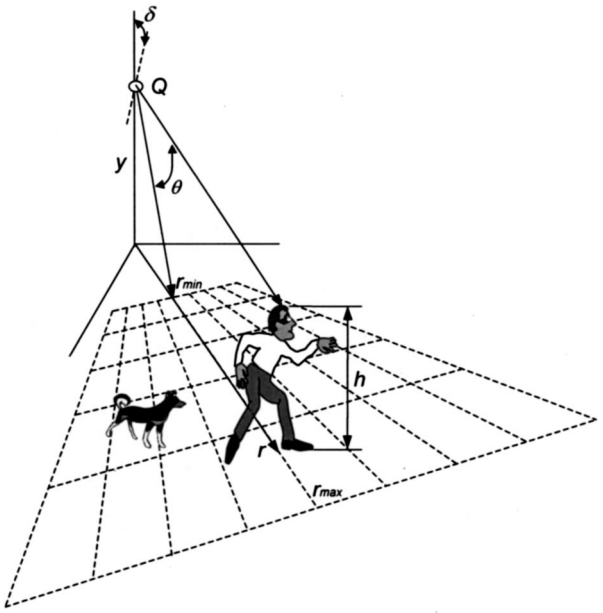

Fig. 1 Optical geometry of an indoor PIR surveillance system.

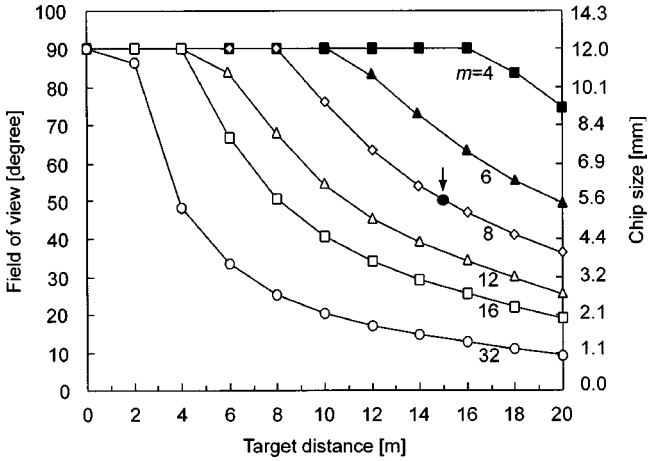

Fig. 2 Calculation of the detection capability of a thermal imaging system with a 64×64 array detector, 6-mm focal length, downward angle of 25 deg, and maximal target height of 1.8 m.

ager. Two image recognition algorithms are utilized to compare the detection probabilities on illustrative human beings and pets. A completely CMOS-compatible process for manufacturing the low-cost micromachined IRFPA microbolometer chip is also proposed and discussed in detail.

2 System Considerations

Figure 1 shows an illustration of the optical environment that generally appears inside a house for PIR security monitoring. The PIR detection system Q is mounted in a corner, close to the ceiling (height y), with a suitable downward-looking angle δ for optimal coverage of the surveillance field, which is characterized by a field of view (FOV) θ and a detection range $r_{\min}$ to $r_{\max}$, the minimum and maximum distances. A system analysis based on the optical geometry is described below.

According to the geometry, the longitudinal length L of the IRFPA detector inside the system Q can be expressed using

$$L = 2\,f \tan\left(\frac{\theta}{2}\right), \tag{1}$$

with f the lens focal length. If N pixels of the detector are included in L, and if a minimum of m pixels is required to provide effective detection of the target images, then it can be shown that

$$\theta = \frac{2N}{m} \tan^{-1}\left(\frac{h\cos\delta}{2r}\right), \tag{2}$$

with a downward-looking angle

$$\delta = \frac{\pi}{2} - \frac{1}{2}\left[\tan^{-1}\left(\frac{r_{\max}}{y-h}\right) + \tan^{-1}\left(\frac{r_{\min}}{y}\right)\right], \tag{3}$$

where h is the target height and r is the floor distance from the camera position.

Figure 2 depicts the calculated results according to the above three equations, assuming that a square detector with $N = 64$ pixels is used. One notes the trade-off between range and FOV existing in these curves. In addition, if a good detection algorithm can be provided for reducing m, the minimal target feature recognizable, then the system will have a better range-FOV product (figure of merit). The solid circle in Fig. 2 shows that when $m = 8$ pixels the system can cover a surveillance field of nearly 15 m in range with a 50-deg FOV. This condition satisfies the requirements for in-house security systems in general and will be used as the case study in this article. One also notes that, for a small (6-mm) focal length, the detector size is then only $\approx 5.6 \times 5.6\,\text{mm}^2$, with a pixel pitch of $\approx 87.5\ \mu$m. Uncooled infrared detectors with this number of pixels and chip size can be fabricated easily at reasonable cost using standard IC processes, as will be discussed later.

For all thermal imaging systems, it is also important to evaluate the minimal detectable temperature of the targets. This can be expressed as follows[18]:

$$\text{NETD} = \frac{4F^2 + 1}{\tau_0 D^*(dW_\lambda / dT|_{\Delta\lambda})}\left(\frac{B}{A}\right)^{1/2}. \tag{4}$$

Here F is the optical f number; A and D^* are the detection area and normalized detectivity; τ_0 is the effective transmittance between wavelengths λ_0 and $\lambda_0 + \Delta\lambda$; W_λ is the spectral radiant emittance within the spectral band (assumed to be that of blackbody radiation); and $dW_\lambda / dT|_{\Delta\lambda}$ is its temperature derivative (the radiation contrast). Finally, B is the system bandwidth, given by $B = f_r N^2/2$, with f_r the frame rate.

A practical system specification based on the above analyses was calculated and is listed in Table 1. It is used for the following illustrative study of an in-house security system. Note that a system NETD of 0.5°C can be obtained using this specification, which is generally qualified for intrusion and fire detection. Since only stationary pictures

Table 1 The system specifications derived for a low-resolution thermal imager used in home security. The value of dW/dT was calculated according to Planck's formula.

Detectable distance	15 m
FOV	50 deg
Target height	1.8 m
Sensor mounting height	2.0 m
Downward-looking angle	25 deg
Focal length	6 mm
Sensor array size	5.6×5.6 mm^2
Sensor resolution	64×64 pixels
f number	0.8
Optical transmittance	0.9
Frame rate	30 Hz
Noise bandwidth	62 kHz
D^* (Ref. 9)	5.5×10^8 cm Hz$^{1/2}$/W
$dW/dT\|_{6-14\ \mu m,300\ K}$	3.7×10^{-4} W/cm^2 K
NETD	0.5°C

will be used for pattern recognition of room-temperature objects, as will be shown later, the NETD can be further improved by relaxing the frame rate suitably.

3 Recognition Simulation on Low-Resolution Images

To maintain low cost, low resolution is critical in designing thermal imagers for home security applications. It is important to devise a good algorithm capable of minimizing the recognizable image size of the targets. This demand can be studied using direct image simulations on real IR images of various resolutions to determine suitable algorithms for reliable detection, as described below.

3.1 *Construction of the Simulated Images*

The low-resolution thermal images to be simulated are not available, due to a lack of suitable instruments. However, for this study they can be generated from original high-resolution radiometric images using the appropriate effective system parameter conversion. The original images can be obtained from a high-resolution (320×240) uncooled thermal imager consisting of FPA microbolometers, which has a built-in temperature-measuring capability. These images then can be converted to different degrees of resolution using downward resampling techniques after gray-level and modulation-transfer-function (MTF) corrections. The image generation follows the process developed by Horger[19] for perception tests, with some modification.

3.1.1 *Gray-level correction*

The radiation energy from an extended target received instantaneously by a detector pixel (i,j) elicits an output voltage expressed as[20]

$$V_h(i,j)=\frac{AR\beta\tau_0}{4F^2}\int_{\lambda_0}^{\lambda_0+\Delta\lambda}W_\lambda\,d\lambda. \tag{5}$$

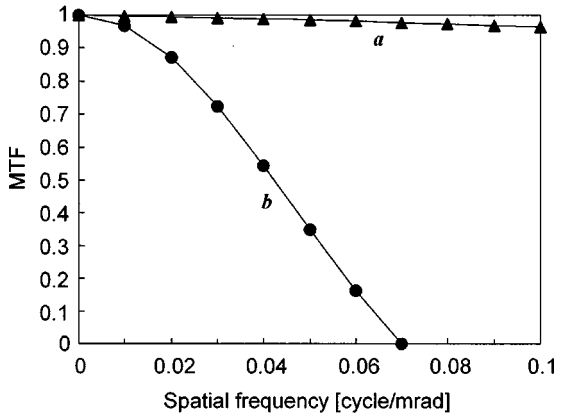

Fig. 3 The system MTF measured on the high-resolution imager for this study (curve *a*) and the numerical calculation for a detector MTF with IFOV=14.6 mrad (curve *b*).

Here R, the detector responsivity, is generally wavelength-independent for thermal detectors, and β is the electronic amplification gain. We have assumed no atmospheric absorption for a short-range security system.

After analog-to-digital conversion, this voltage is quantized into a gray level denoted by $\overline{V}_h(i,j)$ for the corresponding pixel. Except for W_λ, all of the parameters in Eq. (5) could be different for actual low-resolution image systems. If we assume that the electronic parameters and the associated system noise are unchanged, then the gray level of any digitized image, before resampling into various low resolutions, is related to its high-resolution origin by

$$\overline{V}_l(i,j)=\left(\frac{F_h}{F_l}\right)^2\frac{R_lA_l\tau_{0l}}{R_hA_h\tau_{0h}}\overline{V}_h(i,j). \tag{6}$$

This equation, representing the equivalent energy received by two different detection systems, is adopted for the subsequent MTF conversion as a good approximation to a real situation yielding various low-resolution pictures for the simulation experiment.

3.1.2 *MTF correction*

The MTF is taken as the reference for analyzing the resolution conversion. In the spatial frequency domain, the system MTF is the product of individual optic, detector, electronic, and display module MTFs.[21] As depicted in Fig. 3, curve *a* indicates the system MTF measured by the authors on the high-resolution thermal imager used in this study. Shown in the figure is also the one-dimensional MTF of a detector (curve *b*) calculated according to the Lloyd[22] formula,

$$\tilde{r}_d=\mathrm{sinc}(\pi\alpha f_s), \tag{7}$$

with f_s the spatial frequency and α the instantaneous field of view (IFOV). Here α is calculated to be $\approx$14.6 mrad according to the system specification listed in Table 1. Obviously, curve *b* is much lower than curve *a* at high frequency. Hence, it is safe to say that the high-resolution IR images captured for downgrading the conversion can be considered as distortion-free with respect to their original

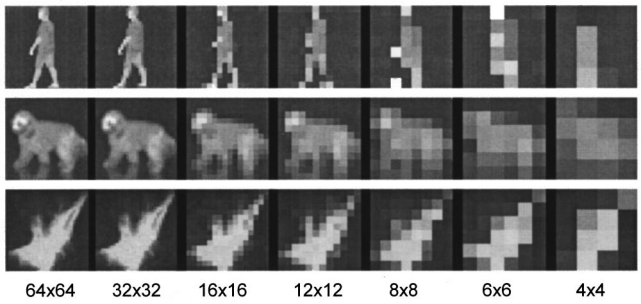

Fig. 4 Illustrations of simulated low-resolution thermal images converted from a high-resolution IR camera.

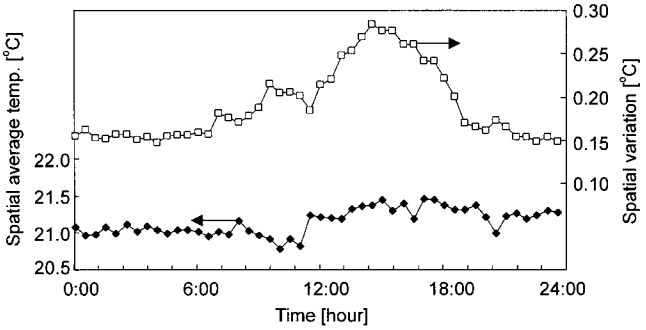

Fig. 5 The spatial average temperature and its standard deviation for an illustrative indoor background over a full day.

scenes, and the converted low-resolution images should be close to those provided by actual low-resolution imaging systems.

In practice, we used the detector spread function in the spatial-domain rather than the frequency-domain MTF to produce the conversion procedure. An image after gray-level correction is convolved with the detector point spread function, using a discrete 2-D method, which is expressed by[23]

$$\overline{V}_{\text{out}}(i,j)=\sum_{m=-k}^{k}\sum_{n=-k}^{k}c(m,n)\overline{V}_{I}(i+m,j+n). \tag{8}$$

Here $c(m,n)$ is the convolution kernel of the point spread function with dimensions $m\times n$, and we have assumed that $m=n=2k+1$ with k depending on the detector IFOV and target distance.

According to the downward resampling technique described here, virtual low-resolution images of varying degrees can be obtained for simulation. Some examples are shown in Fig. 4 for reference. A man, a dog, and a fire were taken as the illustrations for the pattern recognition study.

3.2 *Preprocessing for Image Recognition*

Image preprocessing, including background suppression and data reduction, is important for target feature and speed enhancement. These considerations can be eased by taking a binary representation of the target images with various thresholding techniques.[24,25] However, most techniques generally adopt a single-dynamic-range and limit the pictures to fixed 8-bit gray level. This is not sufficient for the image segmentation of targets with a large intensity range from a common background. Instead, a more efficient method with a dual-dynamic-range and an autothresholding process is proposed for this purpose.

3.2.1 *Dual-dynamic-range process*

A PIR security system should group regular in-house targets into two types according to their relative temperatures: human beings, family pets, and the background as one, and flame and fire, with a much higher temperature, as another. The two types can be easily distinguished from one another using a designated threshold temperature. Hence, at the beginning of target image processing, a wider dynamic range of temperature is set first to detect the possible existence of a high-temperature subject. If the result is positive, then an appropriate algorithm is adopted for fire confirmation. If negative, then the dynamic range is switched to a narrower range for maximizing the difference between the background and potential low-temperature targets. Meanwhile, other algorithms will be used for target identification. Using the dual-dynamic-range procedure, any image before processing recognition will be converted and expanded to its widest gray-level distribution; thus the segmentation between various targets and background can be more complete.

In the following study, the narrow dynamic range is from the exposed human skin temperature (around 32°C)[26] to the room temperature (generally lower). The wide range is upward to 600°C, around the measured burning temperature of a cigarette. These designated ranges, however, may be varied for any user's particular environment.

3.2.2 *Autothresholding*

To extract a target from its background image without numerous computations, background suppression is a necessity before recognition processing. This is achieved by cutting off the part of the image below a certain threshold level, which can be chosen to be slightly above the average temperature ($\overline{T}$) of the background image. If the spatial variation in the background intensity is assumed to be a Gaussian distribution, represented by its standard deviation σ, then one would expect that the background image would nearly vanish after a threshold cut that exceeds $\overline{T}$ by several times σ. This excess temperature can be much greater for fire detection, set in the wide-dynamic-range scheme, so that any low-temperature target image can also be eliminated from the IR picture for a fire check only.

Figure 5 depicts the average temperature $\overline{T}$ over the entire space of a room and its spatial variations. With a $\overline{T}+3\sigma$ threshold value for the background suppression, a human image set in the narrow dynamic range stands out in the picture, as shown in Fig. 6(a) to 6(d). In Fig. 6(b), the peak b (gray level 36) in the histogram is the average background level, and the smaller, higher peak t (level 101) comes from the human. For this picture, σ is calculated to be 11.3; hence the threshold is set at 70. Figure 6(c) shows that the image retained its gray level after the thresholding, while Fig. 6(d) shows its binary image. Notice that the background has been removed completely from the image.

(a)

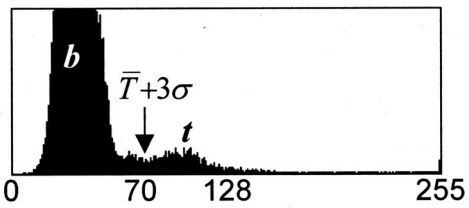

(b)

(c)

(d)

Fig. 6 Image information on a human: (a) as captured; (b) the normalized gray-level histogram; (c) the gray image with a threshold level of 70; (d) the final binary image.

The much simplified image complexion therefore is easier to recognize after autothresholding.

Although 3σ excess is used in this study for the narrow dynamic range, the best choice depends on the background characteristics and can be learned by experience. Also, since $\overline{T}$ and σ are both time-dependent, their values should be automatically and periodically reviewed for better performance when no alarm event occurs.

The dual-dynamic autothresholding (DDAT) treatments mentioned above provide better indoor target images for subsequent recognition with improved speed and accuracy.

3.3 *Target Feature Recognition*

Although there are many choices of algorithms for image recognition, only two were developed in this study. Their detection capabilities are compared with one another to emphasize the importance of the software aspect of PIR image detection in the narrow dynamic range. These two algorithms are the aspect-ratio method and the neural-network method, described below.

The aspect-ratio method utilizes the apparent difference in spatial features between targets that possess the same temperature range. In our case these targets are human beings and family pets. One recognizes that a human shape is upright (taller and slimmer) in comparison with that of pets.

Hundreds of images of persons and dogs in various poses were taken using a high-resolution 8- to 12-μm-wavelength thermal imager, and put in a database. Figure 7 shows examples from the image database. The narrow-dynamic-range and the 3σ autothresholding treatments were applied to obtain the binary images for the aspect-ratio algorithm study. The results are shown in Fig. 8. Here the aspect-ratio feature is defined as the ratio of the greatest vertical to the widest horizontal projection of an image. One notes that in the figure, the human and dog distributions are separated into two groups of histograms, which are obviously distinguishable. A threshold value of ≈ 1.6 in this case can be used for optimal segmentation. However, this value can be varied from case to case without restriction.

The neural network method employed here is a technique that incorporates the self-organizing mapping (SOM) method reported by Kohonen[27] using a multilayer perceptron (MLP).[28] The operation procedures are summarized in Fig. 9. In order to easily form the self-organizing clusters, based on character similarity, it is better to use the continuous-valued input for the SOM method. This means that the gray images after background suppression, such as that shown in Fig. 6(c), should be taken. In Fig. 8, the Kohonen learning (*a*) was operated 1000 times in order to learn the internal cluster rule among these images. Subsequently the MLP network (*b*) was operated with classification matching iterations until the feedback error was below an appointed percentage (0.1% here). Finally, the recognition (*c*) of a human being or dog image was carried out. The error evolution of the MLP network for the different image resolutions is illustrated in Fig. 10. One notes that with an 8×8 feature size ($m=8$), the learning becomes slower, and learning becomes very difficult for a 4×4 array.

For flame or fire detection, only the wide-dynamic-range autothresholding was employed. As mentioned before, this

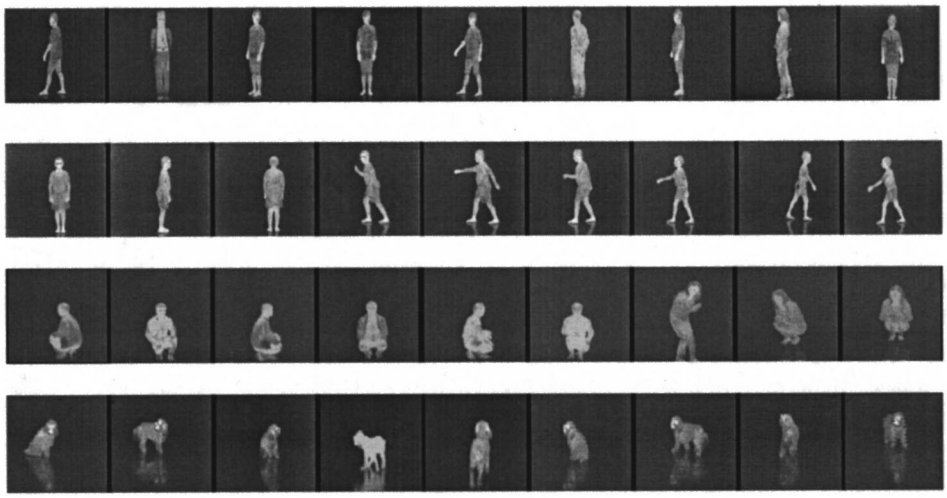

Fig. 7 Examples from the image database used for developing pattern recognition algorithms.

detection was checked at the beginning of a detection cycle. After a positive threshold response, the change in size of a potential flame is monitored immediately and constantly with the correct algorithm for a fire check. Figure 11(a) demonstrates the measurements for an evolving experimental flame in different simulated resolutions. One should note that the image size S of an increasing uncontrolled fire is not steady for low resolutions; hence, the

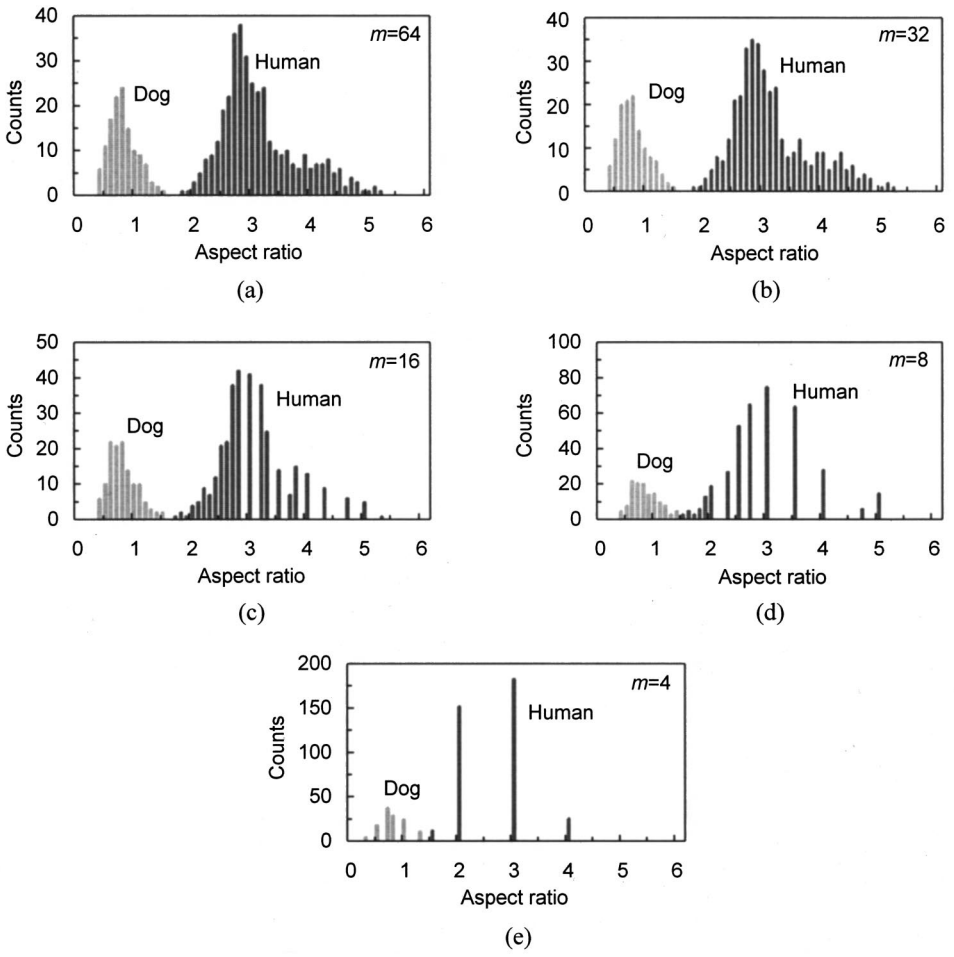

Fig. 8 The aspect-ratio distributions of human beings and dogs with different feature sizes.

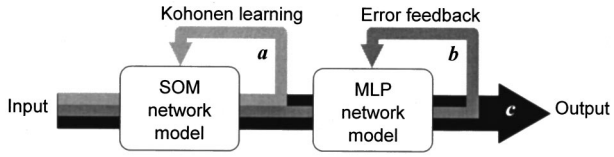

Fig. 9 The neural network model for human and dog recognition.

early fire detection capability is not reliable. This is especially true for the 4×4 feature. In addition, although an initial fire is stationary but expanding, its image size also depends upon its optical distance from the imager; hence it is not practical to identify a fire using its absolute size. To solve this problem, the fractional growth rate relative to the instantaneous size was used. Figure 11(a) is converted into a size-independent plot, as shown by Fig. 11(b), where the increasing rate in logarithmic size, $\mathrm{d}(\ln S)/\mathrm{d}t$, is used for judgement. One can see that, indeed, all curves converge and there is a sufficient margin above zero (cross-hatched) allowed for taking a threshold value to distinguish fire from other sources. One notes that controlled high-temperature objects, such as a lighted cigarette, a fire in a fireplace, or lighted lamps, are all of fixed sizes; therefore no increases in size for these objects is found. Their levels, plotted in Fig. 11(b), will be close to vanishing, and an alarm will not be triggered.

The recognition procedures in this study are summarized by the flow chart in Fig. 12 for reference.

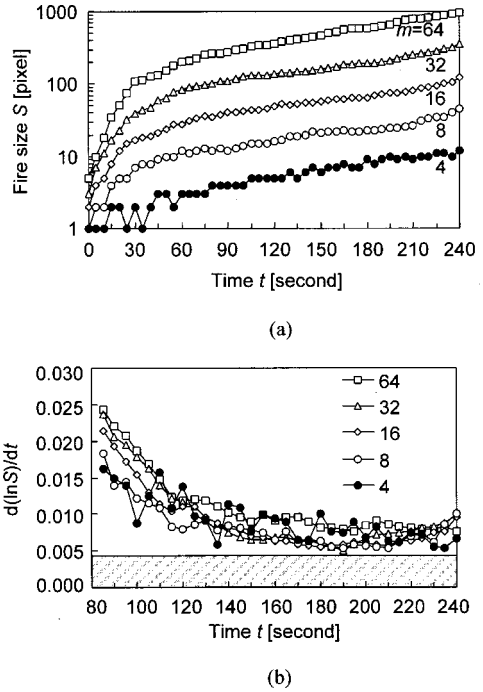

Fig. 11 Evolution behavior of a fire: (a) Temporal size variations with different resolutions. Each datum was taken from one sampling every 5 s. (b) The converted plot from (a) representing the instantaneous fractional growth rate of the fire. Each datum was from an average of 16 sequential samplings over an 80-s duration. The sampling occurred in 5-s steps. Notice that all curves crowd together into a size- and distance-independent behavior.

4 Results and Discussions

4.1 *On the System Design*

The system specifications, including detection range and FOV, are indispensable for the relevant optical and detector design criteria. The relationships shown in Fig. 2 provide useful information for evaluating the system performance for a selected chip size, a focal length, and an array resolution. In the figure, any coordinate in the field region above a curve is beyond the limit of detection at the selected conditions as described by that curve. For example, with a minimal feature size of $m=8$, $f=6$ mm, and $F=1.0$, one can easily find from the figure that the detectable FOV and target distance are limited below 50 deg and $\approx$15 m with an $\approx5.6\times5.6$-mm^2-size detector.

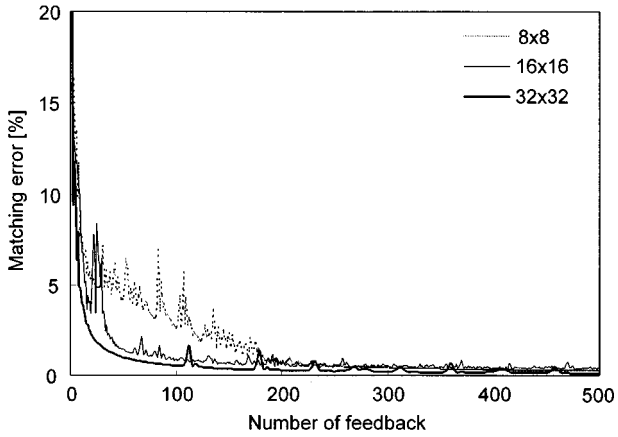

Fig. 10 Error evolution of target classification matching using multilayer perceptron network.

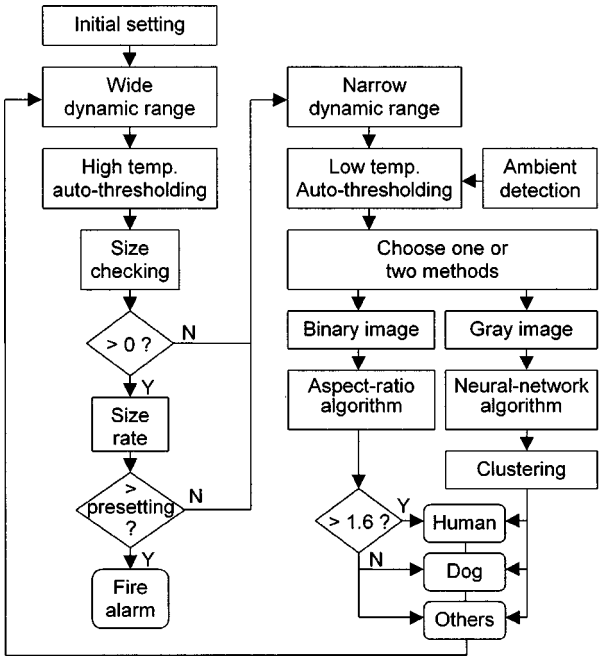

Fig. 12 The flow chart of target recognition in this study.

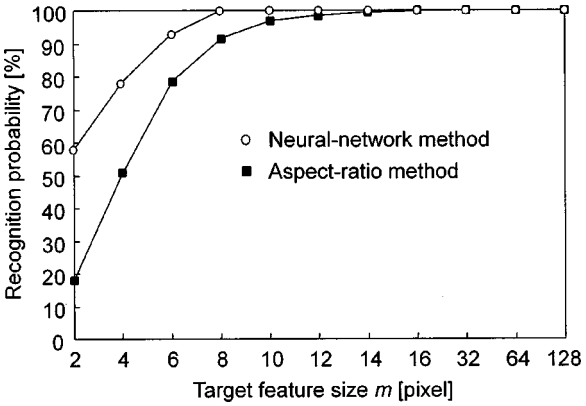

Fig. 13 Recognition probabilities with the neural network and aspect-ratio methods.

Another important factor strongly affecting the performance and manufacturing economy of the detector is the merit of the recognition algorithm. Although the aspect-ratio algorithm is useful for discerning a person from a pet, as illustrated in Fig. 8, due to the small margin existing between the two groups of histograms, the probability of recognition is not 100%. This is manifested by the results of our study shown in Fig. 13. Here, using the aspect-ratio method, the target minimum feature must be over 16×16 pixels in order to have a high detection confidence. Nevertheless, this feature will either greatly reduce the zone of surveillance or increase the costs of the detector chip and optics in the system. The neural network method used in this study not only presents a better result, but is also suitable for any person in various poses, even a squat or crawl. As shown in Fig. 13, the minimum resolvable target size can be reduced to 8×8 pixels for perfect recognition under the same system constraints. Here one should realize that high detection probability is indispensable in security systems. Therefore, it can be concluded that the neural network algorithm is superior to the aspect-ratio algorithm for low-resolution PIR pattern recognition of living objects within a house.

Because of its high temperature, fire can be detected using a wide-dynamic-range scheme with large temperature margins for easily screening the background. To avoid the distance effect in the image and reduce the possibility of false alarm caused by indoor high-temperature objects with fixed size, fire checks should be carried out according to the instantaneous increase in its fractional size. As shown in Fig. 11(a), when the image size is only 4×4 pixels, large fluctuations in the number of pixels appear in the fire image; hence the early detection is not reliable. This fluctuation problem can be decreased with higher resolution. However, with a higher resolution, such as 64×64, the fire size at detection will be too large at a greater distance with the present optical system specification, so that this is not a suitable technique for early fire detection. To solve this problem, multiple samplings over a longer time slot should be used to average out the fluctuation. In our analysis, 16 samplings in an 80-time slot were used for averaging, one sample being taken every 5 s. The result is shown in Fig. 11(b), where a definite clearance (cross-hatched) exists above the zero level, and this can be used for distinguishing an expanding fire from some safe high-temperature objects of fixed size. Thus a 4×4 fire image can be used for early fire detection at 80 s (end of first sampling duration), which means, with the present optical specification, that at a 15-m distance the fire size is only $\approx 30 \times 30\ \mathrm{cm}^2$.

It is also worthwhile to emphasize that the general field requirement for home security, as indicated by Fig. 2, also demands a 64×64 array detector containing an $\approx 5.6 \times 5.6\text{-mm}^2$ size chip with a pixel pitch of $\approx 87.5\ \mu\mathrm{m}$. These requirements can be met using a minimal 8×8 neural detection feature. These sizes are very favorable for cost-effective detector manufacturing.

4.2 *On the System Cost*

To produce a low-resolution PIR image system for home-security applications, it is important that the system have a reasonable price. This is primarily dependent on the fabrication costs of the uncooled IRFPA chip and the associated optics.

4.2.1 *The detector*

Currently, commercial uncooled IRFPA detectors are manufactured by (front-end) silicon IC technologies with an additional (rear-end) surface micromachining process near the end of fabrication.[9] An IRFPA structure must contain an array of floating diaphragms to provide for the support of individual sensors and minimal thermal loss for sensitivity.

Among the types of uncooled IRFPA sensors—pyroelectric,[29,30] thermopile,[31,32] and bolometer[12–15]—the microbolometer is the most promising candidate for our application, for cost reasons. This is because its fabrication is most compatible with standard CMOS processes existing in current foundries. Pyroelectric materials are quite difficult to process in IC foundries due to the potential contamination from nonstandard materials and the processing barriers. Thermopile devices are suitable, but only for simple or linear-array detectors, because of the difficulty of layout geometry in fabricating FPAs. The weak response in thermopile devices is also difficult to manage when it faces the large noise produced by two-dimensional MOS switches, which are associated with an FPA detector.

In order to improve the fill factor for better optical perception, most current microbolometer array detectors are formed in a two-level structure (sensor membrane over on-substrate switches) using the sacrificial-layer technique,[12–15] which is complicated from the process viewpoint. This kind of structure cannot be easily formed using the standard CMOS process steps; thus painstaking and time-consuming process tuning is required within a foundry. This creates a great startup barrier to low-cost voluminous production for new microelectromechanical system (MEMS) companies.

A process flow, which is completely compatible with standard SPDM (single-poly double-metal) CMOS processes, is proposed as shown in Fig. 14. This process allows an uncooled microbolometer IRFPA of single-level structure to be manufactured similarly to a common application-specific IC (ASIC) chip, which a foundry will be willing to produce in limited quantities. One should note

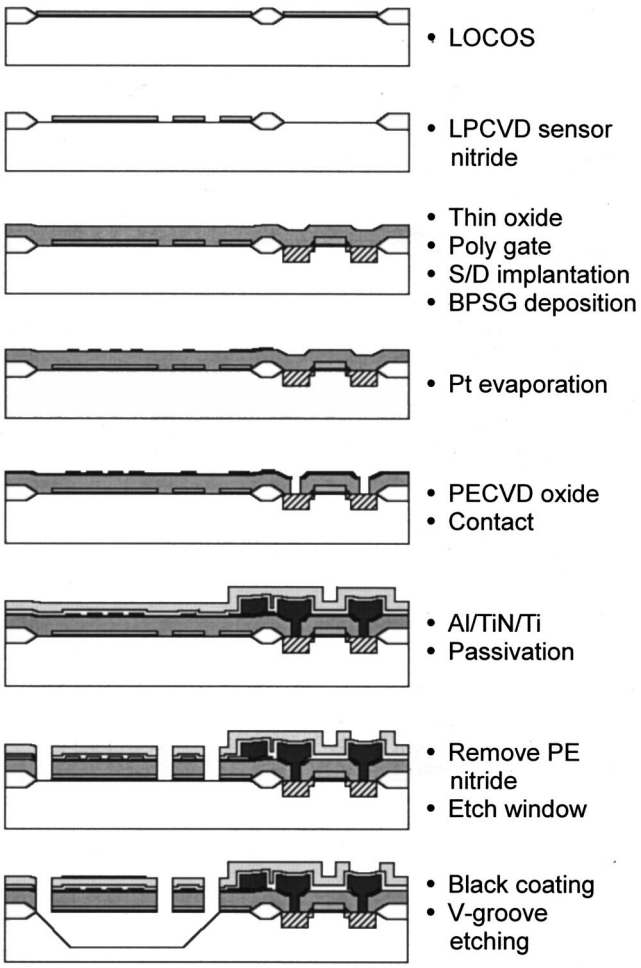

Fig. 14 A proposed monolithic FPA microbolometer fabrication having high compatibility with standard CMOS processes.

that, in this process recipe, the sensor film is totally isolated from other active MOS switches; hence possible direct contamination of the MOS cells is avoided. Furthermore, if materials commonly adopted in silicon IC foundries, such as Ti, silicide, polysilicon, or silicon-germanium, are used for fabricating the bolometer sensor, then the contamination issue is completely avoided. The micromachining step for the floating membrane is last; thus it can be performed off foundry by the MEMS company itself.

The results of this study indicate that the required pixel size is $87.5\times87.5\ \mu m^2$. This area is larger than that of a high-resolution uncooled IRFPA ($\approx50\times50\ \mu m^2$)[14]; hence the fractional area occupied by both the same on-pixel MOS cell and the signal lines is greatly reduced. If finer design rules are adopted for the device process, the fill factor we calculated can be even better ($>70\%$ for an 0.8-μm rule) than these reported values ($\leqslant60\%$) using the sacrificial-layer technique.[12,14]

Figure 15 shows a photograph of the initial device made by the authors according to this process scheme in a local foundry. A very high process yield resulted. It is expected that the cost of the uncooled IRFPA chip with 64×64 resolution will be in the range of a few dollars, which is very favorable for a detector for home security applications.

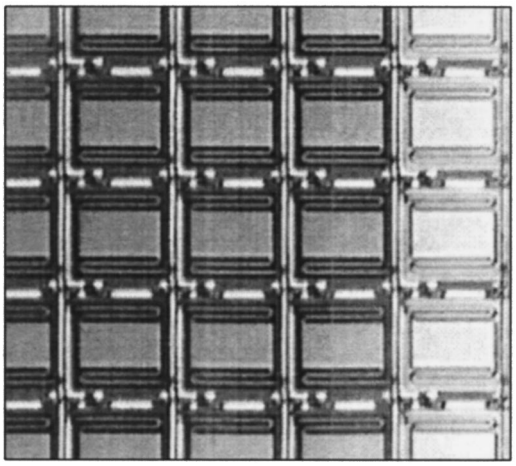

Fig. 15 A fabricated monolithic IRFPA microbolometer. Detectors on the right edge column are dummy sensors for ambient temperature and offset compensation.

4.2.2 *The optics*

When the cost of the IRFPA detector chip is reduced to a certain range, close to the level of ASIC products, the cost of the IR optical components will become the dominating cost factor[33] in a low-resolution thermal imaging system. Hence, it is advisable to consider low-cost lens fabrication in some detail.

There are generally three classes of IR optics for thermal imagers: refractive, reflective, and diffractive,[34,35] in sequence of both performance and cost. However, due to the low-resolution requirement, cost is the most important factor as long as performance requirements are met. Figure 16 shows the MTFs of three qualified commercial IR optics measured in our laboratory. It is interesting to note that the MTF performance of the plastic refractive Fresnel lens is still adequate for use with the 64×64 IRFPA detector that is required by the system specification listed in Table 1.

The Fresnel lens is made of polyethylene plastic plate, and can be produced through a molding process with an expected cost much lower than that of the detector. However, the IR system requires a small lens with 6-mm focal

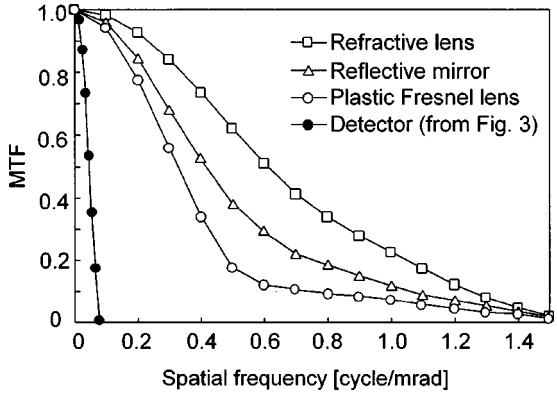

Fig. 16 MTF measurements on different thermal imaging optics. In view of the depicted detector MTF, all three are qualified for this application.

length and *f* number 1.0. Some research is still needed to improve the molding precision to achieve a lens with the demanded quality.

From the above analyses, it can be concluded that a 64 $\times$64 low-resolution, low-cost, uncooled thermal imager can be produced for home-security applications, as judged by the process feasibility and costs required to produce the imager components.

5 Conclusion

Producing low-cost PIR imagers for general home-security applications is feasible by using low-resolution uncooled IRFPA detectors. This study demonstrates that target images with minimum features as low as 8×8 pixels are adequate for highly reliable detection of room-temperature objects using neural network recognition, while a smaller 4×4-pixel image is adequate for early fire detection. For surveillance fields as wide as 50-deg FOV at a range of 15 m, this means that a detector chip contains only 64 $\times$64 pixels at a size of approximately 6×6 mm^2. This small detector chip, together with a proposed high-yield standard CMOS process-manufactured in regular foundries, and with a plastic Fresnel lens, will reduce the system cost to very economical levels.

Although this study utilized stationary picture recognition for human beings and pets, the correlation between sequential motion images should also be used for future study, which could result in an even smaller recognizable feature size. This will then either improve the performance (detection range) or reduce the cost (detector size).

A home security system produced in this way will be affordable to most civilian users. It is expectable that the reliable small uncooled thermal imaging system will exhibit enhanced performance over present PIR detection systems and open an expanded market for the security industry in the future.

Acknowledgment

This work is partially sponsored by the ITRI MEMS program and the National Science Council of Taiwan.

References

1. R. W. Whatmore, ''Pyroelectric devices and materials,'' *Rep. Prog. Phys.* **49**, 1335–1386 (1986).
2. K. Morinaka et al., ''Human information sensor,'' *Sens. Actuators A* **34**, 1–8 (1998).
3. P. Ryser, ''Optical systems for security engineering,'' *Opt. Eng.* **34**(9), 2670–2674 (1995).
4. Nippon Ceramic Corporation, *Pyroelectric Infrared Sensor Technical Information*, Nippon Ceramic Corporation Ltd., Tottori-shi, Japan (1992).
5. J. Grant, *Intruder Alarms*, pp. 112–159, Paramount Publishing, Hertfordshire, UK (1996).
6. M. Constant and P. Turnbull, *The Principles and Practice of Closed Circuit Television*, Chap. 12, Paramount Publishing, Hertfordshire, UK (1994).
7. P. Burry, *Fire Detection and Alarm Systems*, pp. 19–84, Paramount Publishing, Hertfordshire, UK (1996).
8. K. C. Liddiard, ''Thin-film resistance bolometer IR detectors,'' *Infrared Phys.* **24**(1), 57–64 (1984).
9. J. S. Shie and P. K. Weng, ''Design considerations of metal-film bolometer with micromachined floating membrane,'' *Sens. Actuators A* **33**, 183–189 (1992).
10. J. S. Shie et al., ''Characterization and modeling of metal-film microbolometer,'' *IEEE J. Microelectromech. Syst.* **5**(4), 298–306 (1996).
11. D. A. Scribner et al., ''Infrared focal plane array technology,'' *Proc. IEEE* **79**(1), 66–85 (1991).
12. R. A. Wood, ''Uncooled thermal imaging with monolithic silicon focal planes,'' in *Infrared Technology XIX, Proc. SPIE* **2020**, 322–329 (1993).
13. C. Marshall et al., ''Uncooled infrared sensor with digital focal plane array,'' in *Infrared Detectors and Focal Plane Arrays IV, Proc. SPIE* **2746**, 23–31 (1996).
14. A. Tanaka et al., ''Infrared focal plane array incorporating silicon IC process compatible bolometer,'' *IEEE Trans. Electron Devices* **43**(11), 1844–1850 (1996).
15. H. Jerominek et al., ''64$\times$64, 128$\times$128 and 240$\times$320 pixel uncooled IR bolometric detector arrays,'' in *Infrared Technology and Applications XXIII, Proc. SPIE* **3061**, 236–247 (1997).
16. R. E. Flannery and J. E. Miller, ''Status of uncooled infrared imagers,'' in *Infrared Imaging Systems, Proc. SPIE* **1689**, 379–395 (1992).
17. Anon., *U.S. Commercial and Military Infrared System Markets*, Frost & Sullivan (1995).
18. P. W. Kruse, ''Uncooled IR focal plane arrays,'' in *Infrared Technology XXI, Proc. SPIE* **2552**, 556–563 (1995).
19. J. D. Horger, ''Image generation for perception testing using computer flir simulation,'' in *Infrared Imaging Systems: Design, Analysis, Modeling, and Testing, Proc. SPIE* **1309**, 181–189 (1990).
20. R. D. Hudson, *Infrared System Engineering*, Chap. 13, John Wiley & Sons, New York (1969).
21. R. LeBlanc and C. Contini, ''Infrared focal plane array modeling,'' in *Infrared Imaging Systems: Design, Analysis, Modeling, and Testing, Proc. SPIE* **1309**, 27–39 (1990).
22. J. M. Lloyd, *Thermal Imaging Systems*, Chap. 3, Plenum Press, New York (1982).
23. K. R. Castleman, *Digital Image Processing*, Chap. 9, Prentice-Hall, Englewood Cliffs, NJ (1996).
24. R. P. Kruger and W. B. Thompson, ''A technical and economic assessment of computer vision for industrial inspection and robotic assembly,'' *Proc. IEEE* **69**(12), 1524–1538 (1981).
25. P. K. Sahoo et al., ''A survey of thresholding techniques,'' *Comput. Vis. Graph. Image Process.* **41**, 233–260 (1988).
26. R. D. Hudson, *Infrared System Engineering*, Chap. 3, John Wiley & Sons, New York (1969).
27. T. Kohonen, ''The self-organizing map,'' *Proc. IEEE* **78**(9), 1464–1480 (1990).
28. D. E. Rumelhart and J. L. McClelland, ''Learning internal representation by error propagation,'' *Parallel Distributed Process.* **1**, 318–362 (1986).
29. H. Beratan, C. Hanson, and E. G. Meissner, ''Low-cost uncooled ferroelectric detector,'' in *Infrared Detectors: State of the Art II, Proc. SPIE* **2274**, 147–156 (1994).
30. S. G. Porter, R. Watton, and R. K. McEwen, ''Ferroelectric arrays: the route to low cost uncooled infrared imaging,'' in *Infrared Technology XXI, Proc. SPIE* **2552**, 573–582 (1995).
31. T. Kanno et al., ''Uncooled infrared focal plane array having 128 $\times$128 thermopile detector elements,'' in *Infrared Technology XX, Proc. SPIE* **2269**, 450–459 (1994).
32. M. C. Foote and E. W. Jones, ''High performance micromachined thermopile linear arrays,'' in *Infrared Detectors and Focal Plane Arrays, Proc. SPIE* **3379**, 192–197 (1998).
33. Maxtech International, Inc., *Infrared Imaging News*, **5**(2), 1–3 (1999).
34. M. J. Riedl, *Optical Design Fundamentals for Infrared Systems*, Chap. 4, SPIE Optical Engineering Press, Bellingham, WA (1995).
35. W. L. Wolfe, *Introduction to Infrared System Design*, Chap. 11, SPIE Optical Engineering Press, Bellingham, WA (1996).

Tzong-Sheng Lee received his BS degree in physics from National Central University of Taiwan in 1980 and his MS degree in physics from National Tsing Hua University in 1984. Since then, he has worked in Chung San Institute of Science and Technology on electro-optical system design and infrared system simulations. In 1999, he received his PhD degree in electro-optical engineering from National Chiao Tung University. At present, he is a director of the Microsystems Technology Division of the Microsystems Laboratory at the Industry Technology Research Institute.

Jin-Shown Shie is a professor at the Institute of Electro-Optical Engineering of National Chiao Tung University. He earned his BSEE degree from National Cheng Kung University in 1965 and his MSEE degree from National Chiao Tung University in 1968, both in Taiwan. In 1972, he received his PhD degree in materials science from SUNY at Stony Brook, USA. Dr. Shie has been working for the last twenty years on photodetection technologies, from devices to application systems. He is also a consultant to the local industries in these fields. His present research is on microsystem technology.